Neurobiology of Disease 108 (2017) 54–64

Contents lists available at ScienceDirect

Neurobiology of Disease

journal homepage: www.elsevier.com/locate/ynbdi

# Rabphilin 3A: A novel target for the treatment of levodopa-induced dyskinesias

Jennifer Stanic [a,1], Manuela Mellone [a,l,1], Francesco Napolitano [b,c], Claudia Racca [d], Elisa Zianni [a], Daiana Minocci [a], Veronica Ghiglieri [e,f], Marie-Laure Thiolat [g,h], Qin Li [i,j], Annalisa Longhi [a], Arianna De Rosa [b], Barbara Picconi [e], Erwan Bezard [g,h,i,j], Paolo Calabresi [e,k], Monica Di Luca [a], Alessandro Usiello [b,l], Fabrizio Gardoni [a,*]

[a] DiSFeB, Dipartimento di Scienze Farmacologiche e Biomolecolari, Università degli Studi di Milano, 20133, Milano, Italy
[b] Ceinge Biotecnologie Avanzate, Naples, Italy
[c] Department of Molecular Medicine and Medical Biotechnology, University of Naples "Federico II", Naples, Italy
[d] Institute of Neuroscience, Newcastle University, Newcastle upon Tyne NE2 4HH, UK
[e] Laboratorio di Neurofisiologia, Fondazione Santa Lucia, IRCCS, 00143 Roma, Italy
[f] Department of Philosophy, Human, Social and Educational Sciences, University of Perugia, Perugia, Italy
[g] Univ. de Bordeaux, Institut des Maladies Neurodégénératives, UMR 5293, F-33000 Bordeaux, France
[h] CNRS, Institut des Maladies Neurodégénératives, UMR 5293, F-33000 Bordeaux, France
[i] Motac Neuroscience Ltd, Manchester, United Kingdom
[j] Institute of Laboratory Animal Sciences, China Academy of Medical Sciences, Beijing, China
[k] Clinica Neurologica, Università degli studi di Perugia, Ospedale Santa Maria della Misericordia, S. Andrea delle Fratte, 06156 Perugia, Italy
[l] Department of Environmental, Biological and Pharmaceutical Sciences and Technologies, University of Campania, Luigi Vanvitelli, Caserta, Italy

ARTICLE INFO

*Article history:*
Received 1 May 2017
Revised 19 July 2017
Accepted 16 August 2017
Available online 18 August 2017

*Keywords:*
*N*-methyl-D-aspartate receptor
Levodopa-induced dyskinesias
Pharmacological target
Cell-permeable peptides

ABSTRACT

*N*-methyl-D-aspartate receptor (NMDAR) subunit composition strictly commands receptor function and pharmacological responses. Changes in NMDAR subunit composition have been documented in brain disorders such as Parkinson's disease (PD) and levodopa (L-DOPA)-induced dyskinesias (LIDs), where an increase of NMDAR GluN2A/GluN2B subunit ratio at striatal synapses has been observed. A therapeutic approach aimed at rebalancing NMDAR synaptic composition represents a valuable strategy for PD and LIDs. To this, the comprehension of the molecular mechanisms regulating the synaptic localization of different NMDAR subtypes is required.

We have recently demonstrated that Rabphilin 3A (Rph3A) is a new binding partner of NMDARs containing the GluN2A subunit and that it plays a crucial function in the synaptic stabilization of these receptors. Considering that protein-protein interactions govern the synaptic retention of NMDARs, the purpose of this work was to analyse the role of Rph3A and Rph3A/NMDAR complex in PD and LIDs, and to modulate Rph3A/GluN2A interaction to counteract the aberrant motor behaviour associated to chronic L-DOPA administration. Thus, an array of biochemical, immunohistochemical and pharmacological tools together with electron microscopy were applied in this study. Here we found that Rph3A is localized at the striatal postsynaptic density where it interacts with GluN2A. Notably, Rph3A expression at the synapse and its interaction with GluN2A-containing NMDARs were increased in parkinsonian rats displaying a dyskinetic profile. Acute treatment of dyskinetic animals with a cell-permeable peptide able to interfere with Rph3A/GluN2A binding significantly reduced their abnormal motor behaviour.

Altogether, our findings indicate that Rph3A activity is linked to the aberrant synaptic localization of GluN2A-expressing NMDARs characterizing LIDs. Thus, we suggest that Rph3A/GluN2A complex could represent an innovative therapeutic target for those pathological conditions where NMDAR composition is significantly altered.



## 1. Introduction

The control of abnormal movements still represents a therapeutic challenge in the field of Parkinson's disease (PD) and levodopa (L-DOPA)-induced dyskinesias (LIDs; Bastide et al. 2015). Considering that excessive glutamatergic transmission at the corticostriatal synapse and aberrant activation of NMDA-type of glutamate receptors (NMDARs)

* Corresponding author at: Dept. Pharmacological and Biomolecular Sciences, University of Milano, Via Balzaretti 9, 20133 Milano, Italy.
*E-mail address:* fabrizio.gardoni@unimi.it (F. Gardoni).
[1] These authors contributed equally to this work.
**Available online on ScienceDirect (www.sciencedirect.com).**

http://dx.doi.org/10.1016/j.nbd.2017.08.001

exert a central role in the pathogenesis of PD and LIDs (Bastide et al. 2015; Mellone and Gardoni 2013; Errico et al. 2011), a therapeutical approach based on the classical NMDAR antagonists has been investigated. In spite of both preclinical and clinical studies sharing a general agreement on the potential of these compounds to attenuate PD motor symptoms and reduce LIDs, unfortunately, they are mostly not well tolerated by primates. Amantadine, a low-affinity non-competitive antagonist of NMDARs (Kornhuber et al. 1991) has shown a moderate anti-dyskinetic activity (Da Silva-Júnior et al. 2005; Luginger et al. 2000; Ory-Magne et al. 2014; Snow et al. 2000; Wolf et al. 2010; Thomas et al. 2004). Taking into account that changes in the trafficking/subcellular localization of specific NMDAR subunits at the striatal postsynaptic membrane correlates with the motor behaviour abnormalities observed in models of LIDs (Gardoni et al. 2006, 2012) and dyskinetic PD patients (Mellone et al. 2015), an innovative strategy rescuing the physiological subunit composition of synaptic NMDARs may represent the step forward.

Synaptic retention of NMDAR subtypes is controlled by their subunit composition and their interacting proteins. Even if it is well-known that protein–protein interactions govern the synaptic retention of NMDARs (Paoletti et al. 2013), only few studies focused on the mechanisms controlling NMDAR synaptic abundance as a potential pharmacological target in central nervous system disorders (Hill et al. 2012). Remarkably, we recently demonstrated that an increase in synaptic NMDAR GluN2A/GluN2B subunit ratio in the striatum correlates with the motor behaviour abnormalities observed in rat models of PD and LIDs (Gardoni et al. 2006, 2012). These findings were confirmed in the striatum of dyskinetic monkeys and PD patients (Mellone et al. 2015). Moreover, the systemic treatment with a peptide, able to interfere with the interaction between GluN2A and PSD-95, reduces the percentage of parkinsonian rats developing LIDs (Gardoni et al. 2012) and ameliorates the dyskinetic behaviour in L-DOPA-treated MPTP-monkeys (Mellone et al. 2015). Interestingly, the modulation of PSD-95 interaction also with D1 dopamine receptor has been correlated with the onset of a dyskinetic behaviour (Porras et al. 2012) thus suggesting that the activity of scaffolding proteins regulating receptor trafficking/stabilization at the corticostriatal synapse could be considered a putative target for the treatment of dyskinesia in PD patients (Mellone and Gardoni 2013; Gardoni and Di Luca 2015).

Furthermore, we have very recently described Rabphilin-3A (Rph3A) as a new GluN2A-binding partner (Stanic et al. 2015). Rph3A was known as a synaptic vesicle-associated protein involved in the regulation of *exo*- and endocytosis processes at presynaptic sites (Burns et al. 1998). Our work showed that Rph3A is also enriched at dendritic spines where it interacts with both GluN2A C-terminal domain and PSD-95 (Stanic et al. 2015). Rph3A silencing in neurons was able to reduce the surface localization of synaptic GluN2A subunit and NMDAR currents. Moreover, disrupting GluN2A/Rph3A interaction with interfering peptides leads to a decrease of GluN2A levels at dendritic spines (Stanic et al. 2015). These results indicate that GluN2A/Rph3A/PSD-95 trimeric complex promotes GluN2A-containing NMDAR retention at the postsynaptic membrane.

In this frame, here we characterize the role of Rph3A and Rph3A/GluN2A complex in PD and LIDs. In particular, we explored the possibility of interfering with this protein-protein interaction in order to reduce dyskinetic motor behaviour in 6-OHDA-lesioned rats with a dyskinetic profile following chronic L-DOPA treatment.

## 2. Materials and methods

### 2.1. 6-hydroxydopamine (6-OHDA) rat model

Adult male Sprague Dawley rats (125–175 g; Charles River Laboratories, Calco, Italy) were used in this study. Rats were maintained on a 12 h light/dark cycle in a temperature-controlled room (22 °C) with free access to food and water. All procedures were carried out in accordance with the current European Law (2010/6106/EU) and they were also approved by the Italian Ministry of Health (as indicated in D.Lgs. n. 295/2012-A and in D.Lgs. n. 26/2014 - Authorization 327/2015-PR).

Rats underwent a unilateral stereotaxic injection of 6-OHDA (Sigma-Aldrich, St. Louis, MO, USA; 12 μg at 4 μg/μl, rate of injection 0.38 μl/min) in the medial forebrain bundle (MFB; AP: −4.4, L: +1.2; DV: −7.5) as previously reported (Mellone et al. 2015). Two weeks later, the entity of the nigrostriatal lesion was tested with 0.05 mg/kg apomorphine challenge (Sigma-Aldrich; subcutaneous injection, s.c.), and the contralateral turns were counted for 40 min. Animals which performed at least 200 contralateral turns following apomorphine injection were used for the study (Paillé et al, 2010). These rats displayed >95% loss of nigrostriatal fibers and were classified as fully lesioned. The severity of the lesion was also evaluated by Western blot (WB) analysis measuring the striatal levels of tyrosine hydroxylase (TH; #AB152, Millipore).

Fully lesioned rats were treated with 6 mg/kg L-DOPA (Sigma-Aldrich) in combination with 6 mg/kg benserazide (Sigma-Aldrich), 1 s.c injection/day for 14 days. L-DOPA-induced abnormal involuntary movements (AIMs) were evaluated on days 4, 7, 10 and 14 of L-DOPA administration using a highly validated rat AIMs scale (Cenci et al. 1998; Lundblad et al. 2002; Gardoni et al. 2006) and animals were classified as dyskinetic and non dyskinetic. Dyskinetic rats underwent a single stereotaxic injection of 5 nmol TAT-2A40 or 5 nmol TAT-Scr peptides in the striatum ipsilateral to the 6-OHDA lesion (5 μl; rate of injection 0.5 μl/min; AP: +0.2, L: +3.5, DV: −5.7) between days 15 and 16 of L-DOPA treatment. Dyskinetic rats treated only with L-DOPA were used as further control. In all groups, L-DOPA administration was continued for 6 days after TAT cell-permeable peptides (CPPs) injection. To evaluate the effects of these CPPs on LIDs, behavioral assessments (AIMs score) on TAT-2A-40/TAT-Scr-injected rats were carried out in double-blinded conditions the day before the surgery (18 h before CPPs intrastriatal injection, i.s.), on the day of the surgery (6 h after CPPs i.s.) and the following days (30, 78 and 150 h after CPPs i.s.).

Forelimb akinesia was assessed using a modified version of the stepping test (Paillé et al., 2010). Briefly, the experimenter firmly suspended the rat's hindquarters so that the animal supported its weight on its forelimbs. Then, the experimenter moved the rat backwards along the table (0.9 m in 5 s) three consecutive times per session. For each session, the total score calculated was the sum of the number of adjusting steps observed in the three tests (for the contralateral paw). The number of adjusting steps (ratio contralater/ipsilateral forelimbs) were counted as a measure of forelimb akinesia. All sessions were video recorded and analysed by an investigator blinded to the treatment received by the rat.

### 2.2. MPTP monkey model

Captive bred female monkeys (*Macaca mulatta*; Xierin, Beijing, mean weight, 4.2 kg; mean age, 6.1 years) were housed in individual cages under controlled conditions of humidity, temperature, and light. Food and water were available ad libitum, and animal care was supervised by veterinarians skilled in healthcare and maintenance. Experiments were carried out in accordance with European Communities Council Directive of 3 June 2010 (2010/6106/EU) for care of laboratory animals in an Association for Assessment and Accreditation of Laboratory Animal Care–accredited facility. Procedures were approved by the Institute of Laboratory Animal Science ethical committee.

Macaques received daily saline or MPTP hydrochloride injections (0.2 mg/kg, intravenously) until parkinsonian signs appeared as previously described (Porras et al. 2012; Santini et al. 2010; Shen et al. 2015; Urs et al. 2015; Ahmed et al. 2010). Once PD motor signs were stable in MPTP-treated monkeys ($n = 10$), animals were either untreated ($n = 5$) or treated twice daily with individually titrated dose of L-DOPA that provided maximum reversal of parkinsonian motor signs (Madopar, L-DOPA/carbidopa, 4:1 ratio; range, 9–17 mg/kg) ($n = 5$). This dose of L-DOPA, defined as 100% dose, was used for chronic L-DOPA treatment, which lasted for 4 to 5 months until dyskinesia

stabilized as previously described (Porras et al. 2012; Santini et al. 2010; Shen et al. 2015; Urs et al. 2015; Ahmed et al. 2010). The MPTP intoxication protocol, the chronic L-DOPA treatment, the clinical assessments, the terminal procedure and the characterization of the extent of nigrostriatal denervation were conducted as previously published (Porras et al. 2012; Santini et al. 2010; Shen et al. 2015; Urs et al. 2015; Ahmed et al. 2010). As previously reported (Fernagut et al. 2010), DAT binding autoradiography using [$^{125}$I]-(*E*)-N-(3-iodoprop-2-enyl)-2ß-carboxymethyl-3ß-(4′-methylphenyl)-nortropane (Chelatec, France) showed a dramatic and similar reduction (>95%) in all MPTP-treated groups in comparison to control animals (data not shown). Brain patches collected from 300 μm-thick fresh frozen coronal sections containing cortex and caudate-putamen were then further used for qPCR and WB.

### 2.3. Human tissue

Superior frontal gyrus samples from post-mortem brains of non-demented control ($n = 10$) and Parkinson's disease patients ($n = 10$) were obtained from The Netherlands Brain Bank (NBB) of Amsterdam (https://www.brainbank.nl). All tissues were frozen as fast as possible after death. Post mortem delays, age of PD diagnosis, age of death and L-DOPA treatment duration are listed in Table 1. In accordance with the international declaration of Helsinki, the NBB obtained written permission from the donors for brain autopsy and the use of brain material and clinical information for research purposes. All human data were analysed anonymously.

### 2.4. CPPs

TAT-2A-40 peptide corresponding to GluN2A C-terminal domain 1349–1389 (EDSKRSKSLLPDHASDNPFLHTYQDDQRLVIGRCDSDPYKH) fused to the TAT sequence (YGRKKRRQRRR) and corresponding scramble peptide (YGRKKRRQRRR-LDPHSNPLYCPDLYSERFDVSKDHRLDKTKSDH AQDRASIG) were synthetized by Bachem (Bubendorf, Switzerland). Lyophilized CPPs were solubilized in sterile $dH_2O$ to a stock concentration of 1 mM and stored at −20 °C before use.

### 2.5. Antibodies

The following unconjugated primary antibodies were used: mouse monoclonal (mAb) anti-PSD-95 (Neuromab,); rabbit polyclonal (rAb) anti-GluN2A (Sigma-Aldrich,) and mAb anti-α-tubulin (Sigma-Aldrich); rAb anti-DARPP-32 (Cell Signaling Technology); goat polyclonal anti-ChAT (Novus Biologicals); rAb anti-Rph3A (Abcam); mAb anti-Rph3A (ECM biosciences); rAb anti-P-Ser234 Rph3A (Phospho Solutions Aurora); rAb anti-Rab3A (Abcam); CaMKII (Millipore,); Histone H3 (Proteintech); GluA1(Neuromab) e GluA1 P-845 (Millipore).

**Table 1**
Demographic table summarizing the data of patients from which brain samples were obtained; PMD, post mortem delay.

| # | Diagnostic group | Age (years) | PMD (h) | pH liquor | Age of PD diagnosis | L-Dopa treatment duration (y) | Sex |
|---|---|---|---|---|---|---|---|
| 1 | NC | 88 | 7 | 6.76 | | | M |
| 2 | NC | 79 | 6.3 | 6.32 | | | M |
| 3 | NC | 87 | 6.05 | 6.96 | | | M |
| 4 | NC | 88 | 4.43 | 6.17 | | | M |
| 5 | NC | 83 | 5.45 | 6.35 | | | M |
| 6 | NC | 79 | 5.45 | 6.38 | | | M |
| 7 | NC | 90 | 5.45 | 6.35 | | | M |
| 8 | NC | 79 | 6.30 | 6.71 | | | M |
| 9 | NC | 89 | 6.50 | 6.23 | | | M |
| 10 | NC | 83 | 5.15 | 6.60 | | | M |
| 11 | PD | 87 | 3.40 | 6.33 | 66 | 7 | M |
| 12 | PD | 86 | 5.35 | 6.19 | 60 | 25 | M |
| 13 | PD | 83 | 6.20 | 6.71 | 77 | 6 | M |
| 14 | PD | 81 | 5.15 | 6.78 | 60 | 16 | M |
| 15 | PD | 84 | 6.48 | 6 | 76 | 8 | M |
| 16 | PD | 82 | 6.05 | 6.09 | 79 | 3 | M |
| 17 | PD | 81 | 4.30 | 6.42 | 71 | 10 | M |
| 18 | PD | 86 | 7.25 | 6.26 | 70 | 1 | M |
| 19 | PD | 86 | 4.10 | 6.91 | 83 | 2 | M |
| 20 | PD | 86 | 6.15 | 6.33 | 80 | 6 | M |

Abbreviations: NC, non-PD control; PD, Parkinson's Disease patients; PMD, post-mortem delay; y, years; h, hours; PMD, post-mortem delay; M, male.

### 2.6. Quantitative PCR analysis

Total RNA was extracted from animals and post-mortem PD patients by using RNeasy mini kit (Qiagen), according to the manufacturer's instructions. 500 ng of total RNAs of each sample was reverse-transcribed with Transcriptor First Strand cDNA Synthesis Kit (Roche) using and Random Hexamer primer according to the manufacturer's instructions. qRT-PCR amplifications were performed using LightCycler 480 SYBR Green I Master in a LightCycler 480 Real Time thermocycler (Roche).

### 2.7. Triton insoluble postsynaptic fraction (TIF) purification

Triton-insoluble fraction (TIF) was isolated from rat cortex, striatum, hippocampus and cerebellum. This fraction is highly enriched in post-synaptic density proteins and does not contain any presynaptic marker (Gardoni et al. 2006). Samples were homogenized at 4 °C in an ice-cold buffer containing 0.32 M Sucrose, 1 mM Hepes, 1 mM NaF, 0.1 mM phenylmethylsulfonyl fluoride (PMSF), 1 mM MgCl supplemented with protease inhibitors (Complete™, Sigma) and phosphatase inhibitors (PhosSTOP™, Sigma). The homogenate was centrifuged at 1000*g* for 5 min at 4 °C to remove nuclear contamination and white matter. The supernatant was collected and centrifuged at 13,000*g* for 15 min at 4 °C. The resulting pellet (P2 - crude membrane fraction) was resuspended in hypotonic buffer (1 mM Hepes) and centrifuged at 100,000*g* for 1 h at 4 °C. Triton-X-100 extraction of the resulting pellet was carried out at 4 °C for 15 min in 1% Triton-X-100 and 75 mM KCl. The samples were finally centrifuged at 100,000*g* for 1 h at 4 °C and the pellet obtained representing the TIF were resuspended in 20 mM HEPES.

### 2.8. Postsynaptic density (PSD) purification

Postsynaptic densities (PSDs) were isolated from rat striata. Striata were dissected within 2 min from sacrifice and immediately frozen to limit protein degradation. Homogenization was carried out in a glass-Teflon homogenizer (700 rpm) in 4 ml/g of cold 0.32 M sucrose containing 1 mM HEPES, 1 mM MgCl2, 1 mM NaHCO2, and 0.1 mM PMSF (pH 7.4), protease inhibitors (Complete™, Sigma) and phosphatase inhibitors (PhosSTOP™, Sigma). The homogenized tissue was centrifuged at 1000*g* for 10 min. The resulting supernatant (S1) was centrifuged at 13,000*g* for 15 min to obtain a P2 crude membrane fraction. The pellet was resuspended in 2.4 ml/g of 0.32 M sucrose containing 1 mM HEPES, 1 mM NaHCO3, and 0.1 mM PMSF, overlaid on a sucrose gradient (0.85–1.0–1.2 M), and centrifuged at 82,500*g* for 2 h. The fraction between 1.0 and 1.2 M sucrose (synaptosomal plasma membranes, SPM) was removed and diluted with an equal volume of 1% Triton-X-100 and 0.32 M sucrose containing 1 mM HEPES. This solution was spun down at 82,500 g for 45 min. The pellet (PSD1) was resuspended, layered on a sucrose gradient (1.0–1.5–2.1 M), and centrifuged at 100,000*g* at 4 °C for 2 h. The fraction between 1.5 and 2.1 M was removed and diluted with an equal volume of 1% Triton-X-100 and 150 mM KCl. PSD2 were finally collected by centrifugation at 100,000*g* at 4 °C for 45 min and stored at −20 °C until use.

### 2.9. Co-immunoprecipitation assay

50 μg of proteins from P2 - crude membrane fraction were incubated for 1 h at 4 °C in RIA buffer containing 200 mM NaCl, 10 mM EDTA, 10 mM $Na_2HPO4$, 0.5% Nonidet P-40 supplemented with 0.1% sodium

dodecyl sulfate (SDS) and protein A/G-agarose beads (Santa Cruz, Dallas, TX, USA) as pre-cleaning procedure. The beads were then let to sediment at the bottom of the tube and the supernatant was collected. Primary antibodies were added to the supernatant before leaving to incubate overnight at 4 °C on a wheel. Protein A/G-agarose beads were added and incubation was continued for 2 h, at room temperature on a wheel. Beads were collected by gravity and washed three times with RIA buffer before adding sample buffer for SDS–polyacrylamide gel electrophoresis (SDS–PAGE) and the mixture was boiled for 10 min. Beads were pelleted by centrifugation, all supernatants were applied onto 7–12% SDS–PAGE gels

### 2.10. Pre-embedding immunocytochemistry

Sprague Dawley male rats ($n = 3$) of approximately 150–175 g were used. Animals were perfused with 4% paraformaldehyde (PFA) and 0.1% glutaraldehyde in 0.1 M phosphate buffered saline (PBS, pH 7.2), and brain sections (100 μm) were cut on a Leica VT1000S vibratome (Leica Microsystems, Milton Keynes, UK). All procedures were performed according to the requirements of the United Kingdom Animals (Scientific Procedures) Act 1986 and to the current European Law. The immunolabeling method was previously described (Moreau et al. 2010; Piguel et al. 2014). Briefly, the sections were immunolabeled with rAb anti-Rph3A (1:100; ab68857, Abcam), followed by a biotinylated secondary antibody, ABC Elite Kit (Vector Laboratories). The peroxidase reaction was revealed by ImmPACT VIP substrate Kit (Vector Laboratories). Then the sections were osmicated, dehydrated, and flat embedded in Durcupan resin (Sigma-Aldrich). Ultrathin sections (70–90 nm) were countercolored with uranyl acetate and lead citrate. Control experiments, in which the primary antibody was omitted, resulted in no immunoreactivity.

### 2.11. Free-floating immunohistochemistry (IHC)

Adult male rats were perfused with 4% PFA in PBS. The brain was dissected and post-fixed in 4% PFA in PBS for 2 h at 4 °C. Coronal slices (50 μm) containing the striatal region were obtained with Vibratome 1000 Plus Sectioning System (3 M). Brain slices were rapidly washed in PBS (3 × 10 min at RT) and blocked in 0.3% Triton X-100 in PBS (T-PBS) supplemented with 10% normal goat serum or normal donkey serum (NGS or NDS) for 1 h at RT. Coronal slices were then incubated with the appropriate primary antibody in 0.1% T-PBS with 3% NGS or NDS o/n at 4 °C. Brain slices were washed in PBS (3 × 10 min at RT) and incubated with the appropriate Alexa Fluor®-conjugated secondary antibody in 0.1% T-PBS with 3% NGS or NDS for 2 h at RT. Nuclei were stained with the fluorescent dye 4′,6-diamidino-2-phenylindole (DAPI, 1:500,000 in PBS, Thermo Fischer Scientific). Finally, slices were mounted with Fluoromount mounting medium (Sigma-Aldrich) on a Superfrost Plus glass slide (VWR International, Leuven, Belgium). Labelling was visualized with the LSM510 Metasystem Confocal Microscope (Zeiss, Oberkochen, Germany) and AIM 4.2 software (Zeiss) using 40× objective and sequential acquisition setting at 1024 × 1024 pixel resolution.

### 2.12. Corticostriatal slices

Eight-week-old male Sprague-Dawley rats were decapitated and the brain was quickly removed from the skulls. Consecutive corticostriatal slices were cut with Vibratome 1000 Plus Sectioning System (3 M) (270 μm thick). Slices were then pre-incubated in Kreb's buffer (124 mM NaCl, 3.3 mM KCl, 1.2 mM $KH_2PO_4$, 1.3 mM $MgSO_4$, 2.5 mM $CaCl_2$, 20 mM $NaHCO_3$ and 10 mM glucose, continuously equilibrated with 95% $O_2$ and 5% $CO_2$) for 1 h. Then slices were treated with SKF38393 (10 μM) or Ropinirole (100 nM) for 45 min at room temperature continuously equilibrated with 95% $O_2$ and 5% $CO_2$. Control slices were maintained in the vehicle alone. After treatment, striatal areas were carefully isolated from the slices and then frozen on dry ice for molecular studies.

### 2.13. Statistics

Data were analyzsd using GraphPad Prism version 6 (GraphPad Software, La Jolla, CA, USA). Data followed a normal distribution and the significance of the differences was analysed by unpaired two-tailed Student's *t*-test/one-way or two-way ANOVA followed by Bonferroni or Tukey post-hoc tests as appropriate. Details of the statistical analysis applied in this work and the *p* values are given in the Results section and/or in the Figure legends. Data are presented as mean ± SEM.

## 3. Results

### 3.1. Rph3A characterization in the rat striatum

A putative role for Rph3A in central nervous system disorders with alterations in motor behaviour has been put forward (Chung et al. 2009; Dalfó et al., 2004; Smith et al. 2005, 2007). However, only very few studies addressed the expression and the function of Rph3A in the striatum (Chung et al. 2009) and the analysis of Rph3A in specific striatal cell-types as well as its pre/postsynaptic localization in the striatum are lacking. As shown in Fig.1A, a Rph3A protein band is distinctly detectable in the homogenate and Triton-insoluble postsynaptic fractions (TIF) from different rat brain areas, including cortex, striatum, hippocampus and cerebellum. Using a validated subcellular fractionation method (Gardoni et al. 2001, 2006) we purified excitatory postsynaptic densities (PSDs) from rat striatum and we found that Rph3A is enriched in all membrane fractions, including the PSD fractions (Fig. 1B) similar to GluN2A. Conversely, Rab3A, a known Rph3A-interacting protein at the presynaptic terminal (Burns et al. 1998), was present in several subcellular compartments analysed but not in the PSD fractions (Fig. 1B). Moreover, co-immunoprecipitation (co-i.p.) assay showed that, in the striatum, Rph3A interacts with GluN2A subunit and PSD-95, similarly to what has been described in the hippocampus (Fig. 1D; Stanic et al. 2015). Electron microscopy showed the presence of Rph3A in the dendritic shaft of striatal interneurons (Fig. 1C, left panel) and in dendritic spines of medium spiny neurons (MSNs), mainly in proximity of excitatory synapses identified by their PSD (Fig. 1C, right panel). Confocal imaging confirmed striatal Rph3A to be expressed in both MSNs (DARPP-32 positive cells; Fig. 1E) and cholinergic interneurons (ChAT positive cells; Fig. 1F).

### 3.2. Influence of dopamine activation on Rph3A expression, Ser234 phosphorylation and interaction with GluN2A in the postsynaptic compartment.

It has been demonstrated that treatment with D1 but not D2 dopamine receptor agonists leads to a reduction of GluN2A-containing NMDARs in postsynaptic compartment of MSNs (Vastagh et al. 2012). Taking into account the role of Rph3A in the synaptic retention of GluN2A-containing NMDARs (Stanic et al. 2015) we assessed Rph3A involvement in this process. Treatment of corticostriatal slices with D1 agonist SKF38393 (10 μM, 45 min) induced a significant reduction of Rph3A in a Triton-insoluble postsynaptic fraction (TIF) (Fig. 2A; $^{**}p = 0.0069$, SKF38393 versus Control, unpaired Student's *t*-test, $n = 5$) and a concomitant increase of PKA-dependent Rph3A Ser234 phosphorylation (Fig. 2A; $^{**}p = 0.005$, SKF38393 versus Control, unpaired Student's *t*-test, $n = 4$). These results were correlated with a decreased interaction with GluN2A (Fig. 2B; $^{***}p = 0.001$, SKF38393 versus Control, unpaired Student's *t*-test; $n = 5$). Interestingly, this effect is specific to D1 receptor activity as no change in Rph3A synaptic localization and interaction with GluN2A was observed after treatment with D2 receptor agonist Ropirinole (100 nM, 45 min) (Fig. 2C–D; Rph3A WB in TIF: $p = 0.4769$, Ropirinole versus Control, unpaired Student's *t*-test, $n = 5$; P-Ser234-Rph3A WB in TIF: $p = 0.6810$, Ropirinole versus Control, unpaired

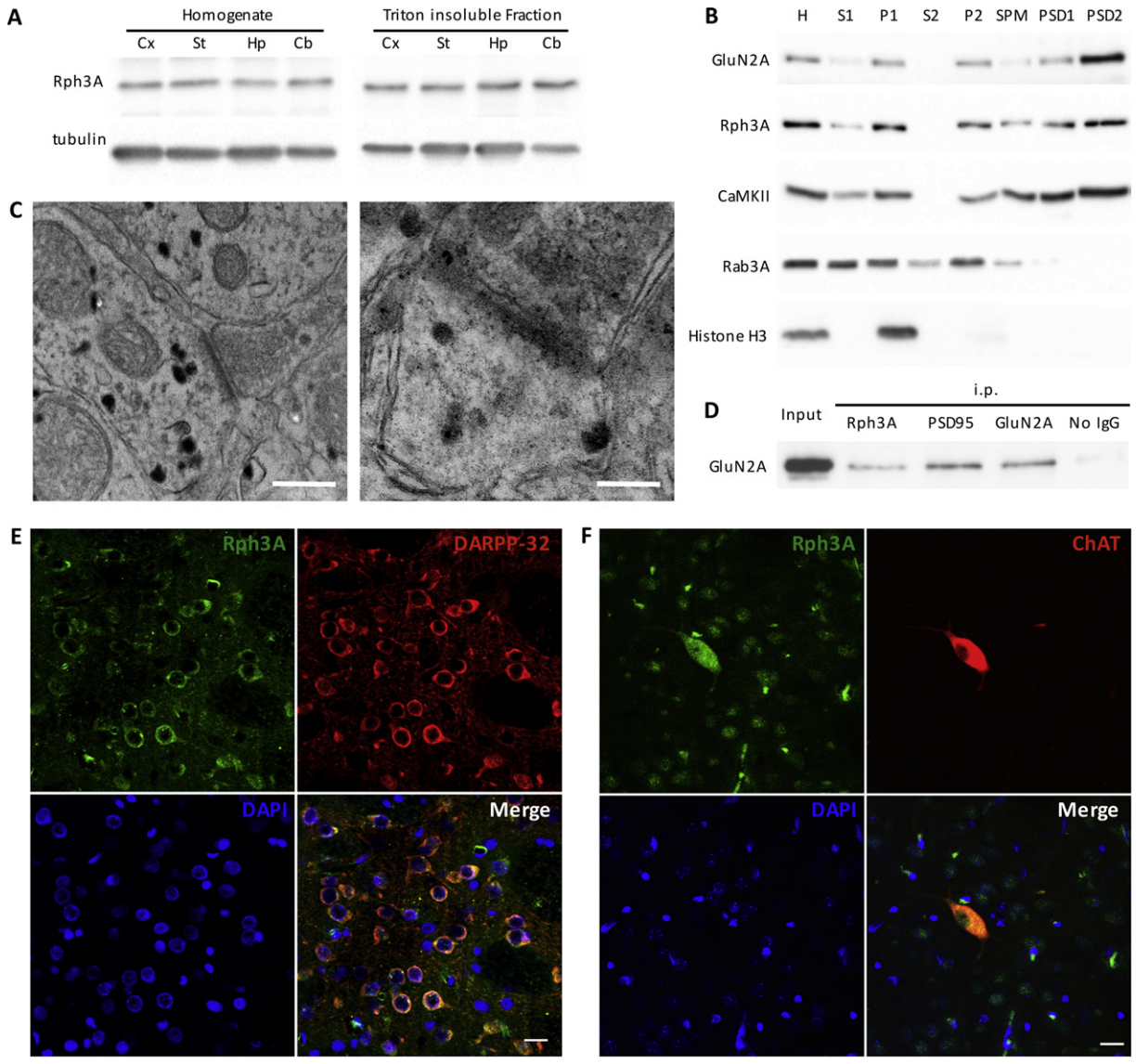


**Fig. 1.** Characterization of Rph3A in rat striatum. (A) Western blot (WB) of Rph3A in homogenate and TIF fractions from different brain areas: Cx, cortex; St, striatum; Hp, hippocampus; Cb, cerebellum. (B) Subcellular expression of GluN2A, Rph3A, CaMKII, Rab3A and Histone H3 in rat striatum. H, homogenate; S1/2, supernatant 1/2; P1/2, pellet 1/2; SPM, synaptosomal plasma membrane fraction; PSD1/2, postsynaptic density fraction 1/2. (C) Immunolabeling of Rph3A in aspiny dendrites of interneurons (left panel) and spines of medium spiny neurons (right panel). Electron microscopy image shows that Rph3A is found in the dendritic shaft of interneurons (left panel) and in spines of spiny neurons (right panel), as well as in proximity of excitatory synapses identified by their PSD. Scale bar: 335 nm (left panel), 200 nm (right panel). (D) Co-immunoprecipitation experiments on rat striatal TIF fractions using polyclonal GluN2A, monoclonal PSD-95 and polyclonal Rph3A antibodies show that GluN2A interacts with Rph3A also in the striatum. (E) Immunohistochemistry for Rph3A (green) and DARPP-32 (MSN marker, red) in the adult rat striatum. Nuclei were visualized with DAPI (blue). Rph3A co-localizes with DARPP-32$^{+}$ cells. Scale bar, 10 μm. (F) Immunofluorescence for Rph3A (green) and ChAT (cholinergic interneuron marker, red) in the adult rat striatum. Nuclei were labeled with DAPI (blue). Rph3A is also co-localizing with ChAT$^{+}$ cell. Scale bar, 10 μm.

Student's *t*-test, $n = 5$; co-ip GluN2A/Rph3A: $p = 0.1651$, Ropirinole versus Control, unpaired Student's *t*-test, $n = 5$).

### 3.3. Rph3A expression in rat, monkey models of PD and human patients with PD

Considering the involvement of Rph3A in the synaptic stabilization of GluN2A-containing NMDARs in the hippocampus (Stanic et al. 2015) and the exacerbated postsynaptic localization of these receptor subtypes in several experimental models of LIDs as well as in parkinsonian patients expressing dyskinesias (Mellone et al. 2015), we evaluated *Rph3A* mRNA and protein levels in PD patients (Table 1) and PD animal models. *Rph3A* mRNA and protein expression levels were unchanged in the whole striatal lysates from dopamine-denervated and dyskinetic rats (Fig. 3A; mRNA: $F_{(2,9)} = 1.539$, $p = 0.2661$; protein: $F_{(2,9)} = 0.3209$, $p = 0.7335$, one-way ANOVA), while MPTP-treated monkeys exhibited a significant reduction of *Rph3A* mRNA levels in caudate putamen, medial and superior frontal gyrus (Fig. 3B upper panels; caudate putamen: $F_{(2,12)} = 5.098$, $p = 0.0250$, one-way ANOVA; CTRL vs MPTP group: $p = 0.0383$, Fisher's post-hoc comparison; medial frontal gyrus: $F_{(2,12)} = 9.167$, $p = 0.0038$; CTRL vs MPTP group: $p = 0.0158$; superior frontal gyrus: $F_{(2,12)} = 4.759$, $p = 0.0301$; CTRL vs MPTP group: $p = 0.0189$). In addition, *Rph3A* mRNA levels were also significantly reduced in the caudate putamen and medial frontal gyrus of parkinsonian monkeys treated with L-DOPA (caudate putamen: CTRL vs MPTP + L-DOPA group: $p = 0.0303$; medial frontal gyrus: $p = 0.0066$, Fisher's post-hoc comparison, $n = 5$), with a trend toward a reduction also in the superior frontal gyrus ($p = 0.0691$). On the contrary, we did not observe a main effect of the lesion, alone or in associated with L-DOPA supplementation, on Rph3A protein levels in the aforementioned brain areas from parkinsonian and dyskinetic monkeys (Fig. 3B lower panels, $p \geq 0.05$, for all analysed groups, $n = 5$). In line with these observations, a significant

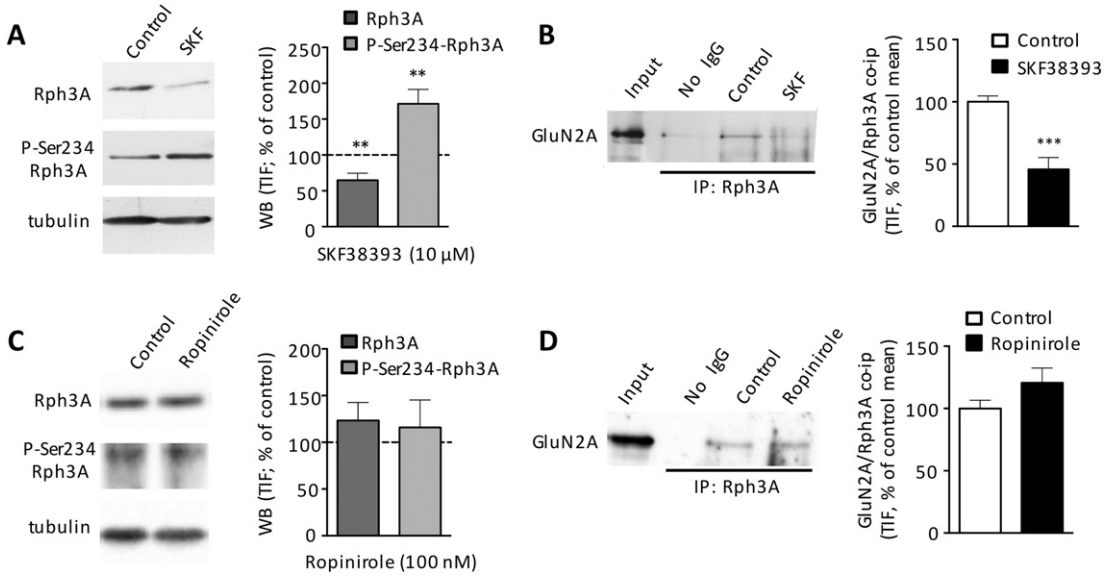


**Fig. 2.** Influence of dopaminergic pathway on Rph3A postsynaptic localization and its interaction with GluN2A. (A) WB analysis of Rph3A, P-Ser234-Rph3A and tubulin from the striatal TIF fraction obtained from control (C) and SKF38393-treated (10 μM, 45 min) corticostriatal slices. The same amount of protein was loaded in each lane. The bar graph shows the amount of Rph3A and P-Ser234-Rph3A in the TIF fraction from SKF38393-treated slices (*t*-test; $^{**}p < 0.01$; $^{*}p < 0.05$). (B) Total homogenate was immunoprecipitated (i.p.) with antibody against Rph3A and the presence of GluN2Ain the immunocomplex was evaluated by Western blot. Treatment with SKF38393 reduces GluN2A co-precipitation with Rph3A (*t*-test; $^{***}p < 0.001$). (C) WB analysis of Rph3A, P-Ser234-Rph3A and tubulin from the striatal TIF fraction obtained from control and ropinirole (100 nM, 45 min) corticostriatal slices. The same amount of protein was loaded in each lane. The bar graph shows the amount of Rph3A and P-Ser234-Rph3A in the TIF fraction from ropinirole-treated slices. (D) Total homogenate was immunoprecipitated (i.p.) with antibody against Rph3A and the presence of GluN2A in the immunocomplex was evaluated by Western blot. Treatment with ropinirole does not modify GluN2A co-precipitation with Rph3A.

reduction in *Rph3A* mRNA, but not protein levels was found in the superior frontal gyrus of post-mortem brain samples from PD patients (Fig. 3C, $p = 0.0498$, Mann-Whitney test, $n = 10$). Overall, these results demonstrate no alterations of Rph3A protein levels in the total striatal lysates from experimental models of PD and LID as well as in PD patients.

### *3.4. Rph3A synaptic localization and interaction with GluN2A-containing NMDARs in the rat model of PD and L-DOPA-induced dyskinesia.*

Taking into account that Rph3A plays a key role in the postsynaptic compartment in the stabilization of GluN2A-containing NMDARs (Stanic et al. 2015), we evaluated its postsynaptic localization and the formation of Rph3A/GluN2A complex. WB analysis performed in the rat striatal postsynaptic fraction revealed an increased synaptic localization of Rph3A in L-DOPA-treated dyskinetic rats (Fig. 4A, left graph; $F_{(2,33)} = 3.736$, $p = 0.0348$, one-way ANOVA, Tukey's post-hoc comparison; DYS versus Control, $^{*}p \leq 0.05$). In addition, a significant decrease in Rph3A Ser234 phosphorylation at synapses was found in dyskinetic animals compared to controls (Fig. 4A, right graph; $F_{(2,18)} = 4.048$, $p = 0.0453$, one-way ANOVA, Tukey's post-hoc comparison; DYS versus Control, $^{*}p \leq 0.05$). This phosphorylation is known to reduce the affinity of Rph3A for membranes regulating its subcellular localization (Fykse et al. 1995; Foletti et al. 2001). Finally, co-immunoprecipitation in striatal homogenates from control, parkinsonian and dyskinetic rats showed augmented GluN2A/Rph3A interaction in the dyskinetic experimental group (Fig. 4B; $F_{(2,24)} = 13.39$, $p = 0.0004$, one-way ANOVA, Tukey's post-hoc comparison; DYS versus Control, $^{***}p \leq 0.001$; DYS vs 6-OHDA, $^{*}p \leq 0.05$).

### *3.5. Modulation of Rph3A/GluN2A complex in L-DOPA treated dyskinetic rats.*

The above results show an increase of Rph3A synaptic levels and its interaction with GluN2A in L-DOPA-treated dyskinetic rats, thus providing a novel molecular mechanism responsible for the aberrant GluN2A synaptic abundance which characterize experimental models of LIDs and dyskinetic PD patients (Gardoni et al. 2012; Mellone et al. 2015). We previously characterized a cell-permeable peptide (TAT-2A-40) able to interfere GluN2A/Rph3A complex by competing with GluN2A for the binding to Rph3A (Stanic et al. 2015). In hippocampal neurons, this disruption by TAT-2A-40 leads to a reduction in GluN2A-containing NMDARs at the synaptic plasma membrane (Stanic et al. 2015). We therefore hypothesized that TAT-2A-40 could be useful to reduce synaptic GluN2A in dyskinetic rats potentially blocking abnormal motor behaviour (see experimental schedule in Fig. 5). To this, we first confirmed by co-immunoprecipitation assay the capability of TAT-2A-40 to disrupt GluN2A/Rph3A interaction following intrastriatal injection. We observed a significant reduction of the GluN2A/Rph3A complex after TAT-2A-40 injection compared to the control scramble peptide in naïve rat striata (Fig. 6A; $^{*}p = 0.0107$, TAT-2A-40 versus TAT-Scr, $n = 3$) as well as in dyskinetic rat ipsilateral striata (Fig. 6B; $^{*}p = 0.0358$, TAT-2A-40 versus TAT-Scr, $n = 7$). We then evaluated whether acute administration of TAT-2A-40 to dyskinetic rats after chronic treatment with L-DOPA could have beneficial effects on their abnormal motor behaviour. TAT-2A-40 ($n = 8$; 5 nmol) or TAT-Scr control ($n = 8$; 5 nmol) peptides were stereotaxically injected in the ipsilateral striatum of 6-OHDA-lesioned rats chronically treated with L-DOPA and displaying dyskinetic motor behaviour (Fig. 5). A group of dyskinetic animals continued the treatment with L-DOPA alone ($n = 6$). Peptides were injected 6 h before the daily L-DOPA administration and the evaluation of AIMs was carried out from 20 to 140 min after L-DOPA (Fig. 6C–G). TAT-2A-40 was able to induce a significant reduction of the AIMs score compared to TAT-Scr control group as well as the untreated dyskinetic group the effect lasting until 150 h after injection (Fig. 6C–G). Moreover, the time course of AIMs development showed that TAT-2A-40 significantly decreased AIMs induction measured during the sessions taking place 6 h (Fig. 6E), 30 h (Fig. 6F) and 150 h (Fig. 6G) after surgery. No differences were observed in rats treated with TAT-Scr control peptide compared to untreated dyskinetic rats, thus demonstrating the absence of any effect induced by the surgery procedure or by the TAT-Scr moiety (Fig. 6C–G). Moreover, no change was induced by TAT-2A-40 or TAT-Scr on the anti-parkinsonian effect of the L-DOPA treatment as evidence by the stepping test, a well-known motor task used to assess motor function, performed on these animals (Fig. 6H).

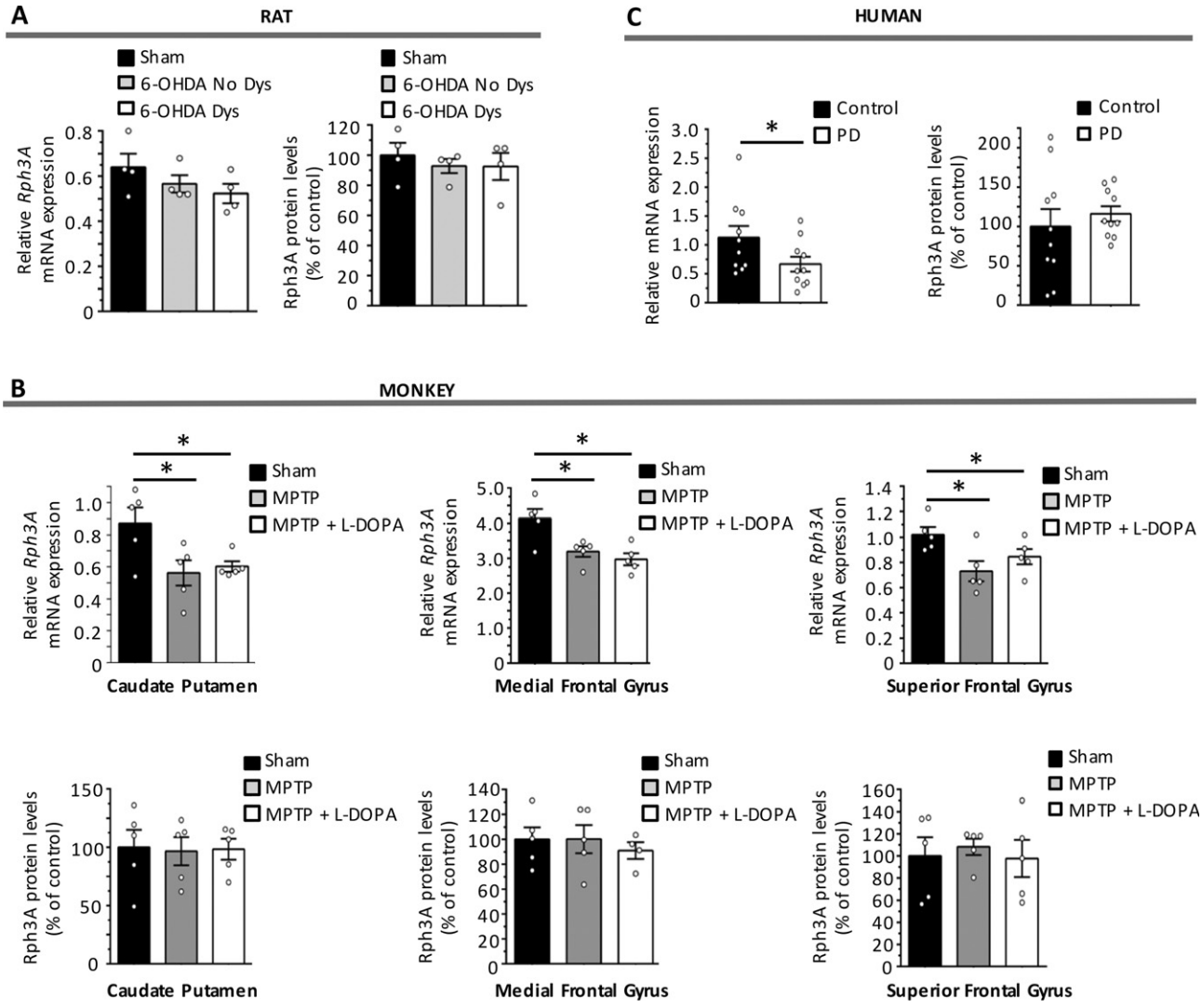


**Fig. 3.** Rph3A expression levels in parkinsonian animal models and PD patients. (A) Striatal *Rph3A* mRNA (left) and protein (right) levels were analysed in 6-OHDA-lesioned rats, with or without dyskinesias ($n = 4$). (B) *Rph3A* mRNA (upper) and protein (lower) expression levels in the homogenates of Caudate Putamen, Medial Frontal Gyrus and Superior Frontal Gyrus from MPTP-treated monkeys, with or without L-DOPA supplementation ($n = 5$). (C) Evaluation of *Rph3A* mRNA (left) and protein (right) levels in the Superior Frontal Gyrus of post-mortem PD patients from the Netherlands Brain Bank ($n = 10$).

Finally, we measured the capability of TAT-2A-40 to reduce the phosphorylation of Ser845-GluA1 subunit of the AMPA receptor as well-known molecular marker of LIDs at the glutamatergic striatal synapse (Ghiglieri et al. 2016). As shown in Fig. 6I, TAT-2A-40 treatment decreased the phosphorylation levels of this AMPA receptor phosphosite compared to TAT-Scr (*$p = 0.0474$, TAT-2A-40 versus TAT-Scr, $n = 7$), indicating a normalization of this molecular marker of dyskinesia correlated to the PKA activity downstream D1 dopamine receptor (Santini et al. 2010).

## 4. Discussion

Among the modifications of the striatal glutamatergic synapse involved in L-DOPA-induced dyskinesia, several reports demonstrated changes in NMDAR activity and subunit composition at MSNs dendritic spines (Gardoni and Di Luca 2015; Bastide et al. 2015). In particular, our previous studies clearly showed a direct correlation between an increase GluN2A/GluN2B ratio at the corticostriatal synapse and the onset of the abnormal involuntary movements both in animal models and in PD patients (Gardoni et al. 2006, 2012; Mellone et al. 2015).

Here we demonstrate that Rph3A plays a key role in the aberrant synaptic localization of GluN2A-containing NMDARs in L-DOPA-induced dyskinesias. In particular, we demonstrate that interfering with Rph3A/GluN2A/PSD-95 complex at the synapse is strategic to correct the aberrant synaptic localization of GluN2A-containing NMDARs. Different experimental approaches revealed that Rph3A is enriched at the corticostriatal synapse where it interacts with the GluN2A subunit. Notably, Rph3A expression at the postsynaptic density and its interaction with GluN2A were increased in parkinsonian rats displaying a dyskinetic profile. Treatment of dyskinetic rats with a cell-permeable peptide able to disrupt Rph3A/GluN2A interaction dramatically reduced the L-DOPA-induced abnormal motor movements. Accordingly, Rph3A/GluN2A complex could represent an innovative therapeutic target for pathological conditions where NMDAR composition is significantly altered such as PD and LIDs (Gardoni et al. 2006, 2012; Mellone et al. 2015).

Alterations in Rph3A immunoreactivity in different types of neurodegenerative disorders (Chung et al. 2009; Dalfó et al., 2004; Smith et al. 2005, 2007; Tan et al. 2014), including α-synucleinopathy, Alzheimer's disease and Huntington's disease have been previously observed. In particular, these reports converge in indicating a downregulation of Rph3A expression in different in vitro and in vivo models of neurodegeneration. We now show that Rph3A mRNA but not total protein levels in striatum is downregulated in PD monkey model as well as in postmortem tissue

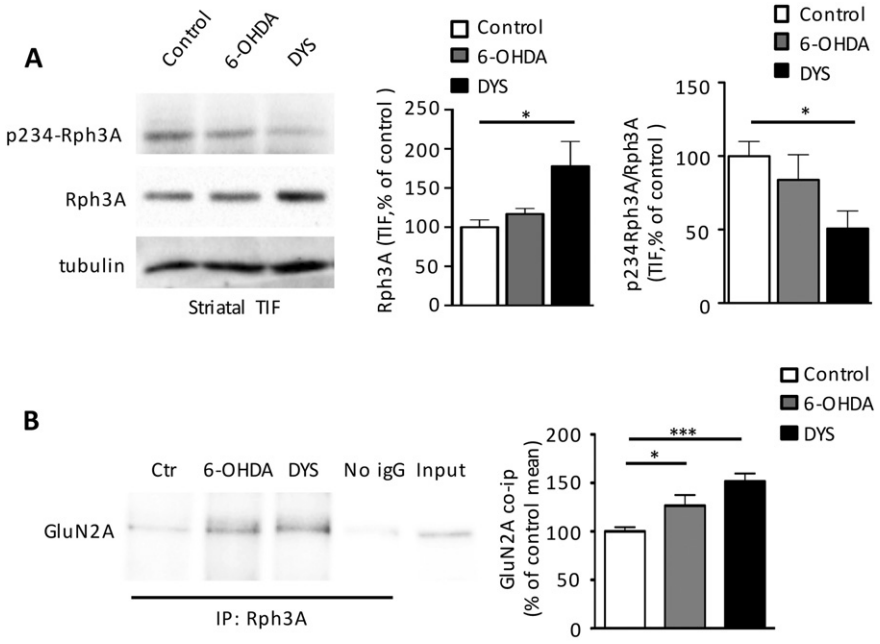


**Fig. 4.** Rph3A phosphorylation, synaptic localization and interaction with GluN2A in the rat experimental model of PD and LIDs (A) WB for Rph3A, pSer234-Rph3A and tubulin of striatal TIF samples from the ipsilateral (6-OHDA) and the contralateral (Control) striata of 6-OHDA-lesioned rats and the ipsilateral striatum of L-DOPA-treated (6 mg/kg/die) dyskinetic animals (DYS). Rph3A and pSer234-Rph3A levels at synapses are altered in dyskinetic rats ($^{*}p \leq 0.05$). (B) Co-immunoprecipitation of GluN2A and Rph3A in P2 fractions from the ipsilateral (6-OHDA) and the contralateral (Control) striata of 6-OHDA-lesioned rats and the ipsilateral striatum of L-DOPA-treated (6 mg/kg/die) dyskinetic rats (DYS) ($^{***}p < 0.001$, $^{*}p < 0.05$).

from PD patients. Interestingly, these alterations were not observed in the rat model of PD thus indicating the existence of a species-specific effect with alterations of Rph3A expression being more evident in primates. In particular, our data suggest a slow modulation of mRNA levels following disease progression and chronic treatment with L-DOPA. Accordingly, we observe an alteration of Rph3A mRNA levels only after a long disease progression and a long-term exposure to the drug as in monkeys and human patients but not in the rat model, characterized by a shorter time schedule of disease and treatment.

Our results show that chronic L-DOPA treatment leading to dyskinesia and pathological plasticity at the corticostriatal synapse (Calabresi et al. 2016) leads to an increased accumulation of Rph3A at the postsynaptic membranes and to a consequent enhanced Rph3A/GluN2A interaction. Several putative mechanisms could explain these molecular alterations. It is well-known that the onset of dyskinesia is linked to a sequence of events that include pulsatile stimulation of DA receptors, changes in downstream signalling pathways and abnormalities in non-DAergic transmitter systems (the glutamatergic synapse), all of which converge to produce aberrant firing patterns that signal between the basal ganglia and the cortex (Bastide et al. 2015). Among other mechanisms, sensitized D1 receptor signalling is required for LIDs onset, even if the specific role of the different molecular components downstream D1 receptor still needs to be clarified (Bastide et al. 2015). In particular, recent studies suggest that Phospholipase C (PLC) can mediate some of the effects of D1 receptor activation (Medvedev et al. 2013) and mGluR5/PLC/PKC cascade can contribute as a potent modulator of D1 receptor activation in the DA-denervated striatum without altering D1-induced PKA activity (Fieblinger et al. 2014). In

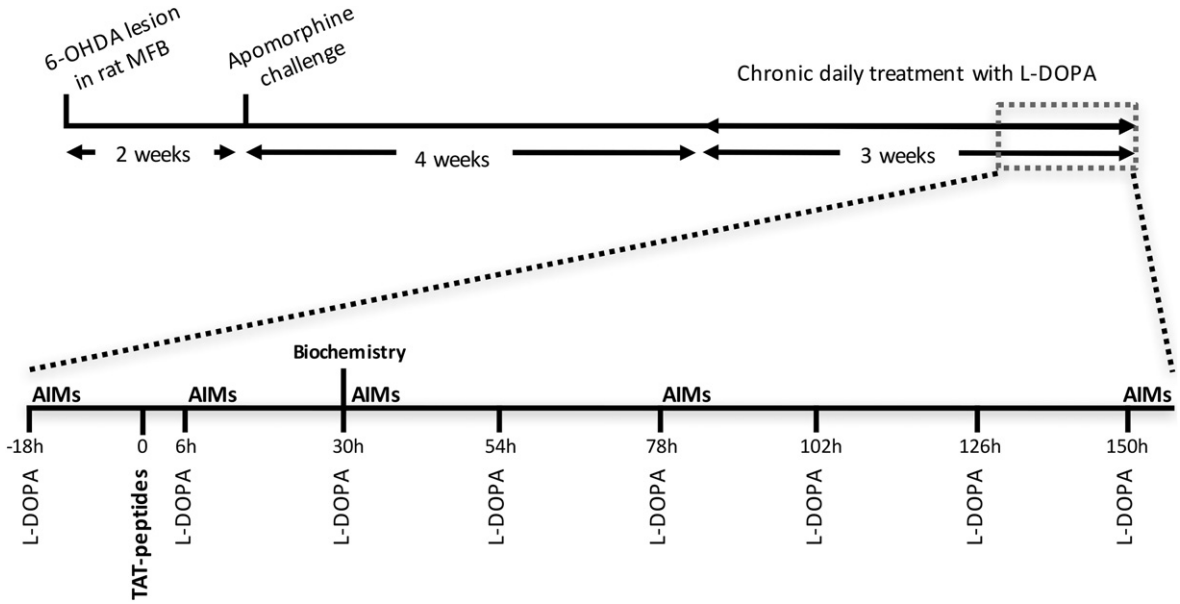


**Fig. 5.** Schematic representation of the experimental plan applied for the injection of TAT-2A-40 and TAT-Scr peptides in 6-OHDA-lesioned rats chronically treated with L-DOPA.

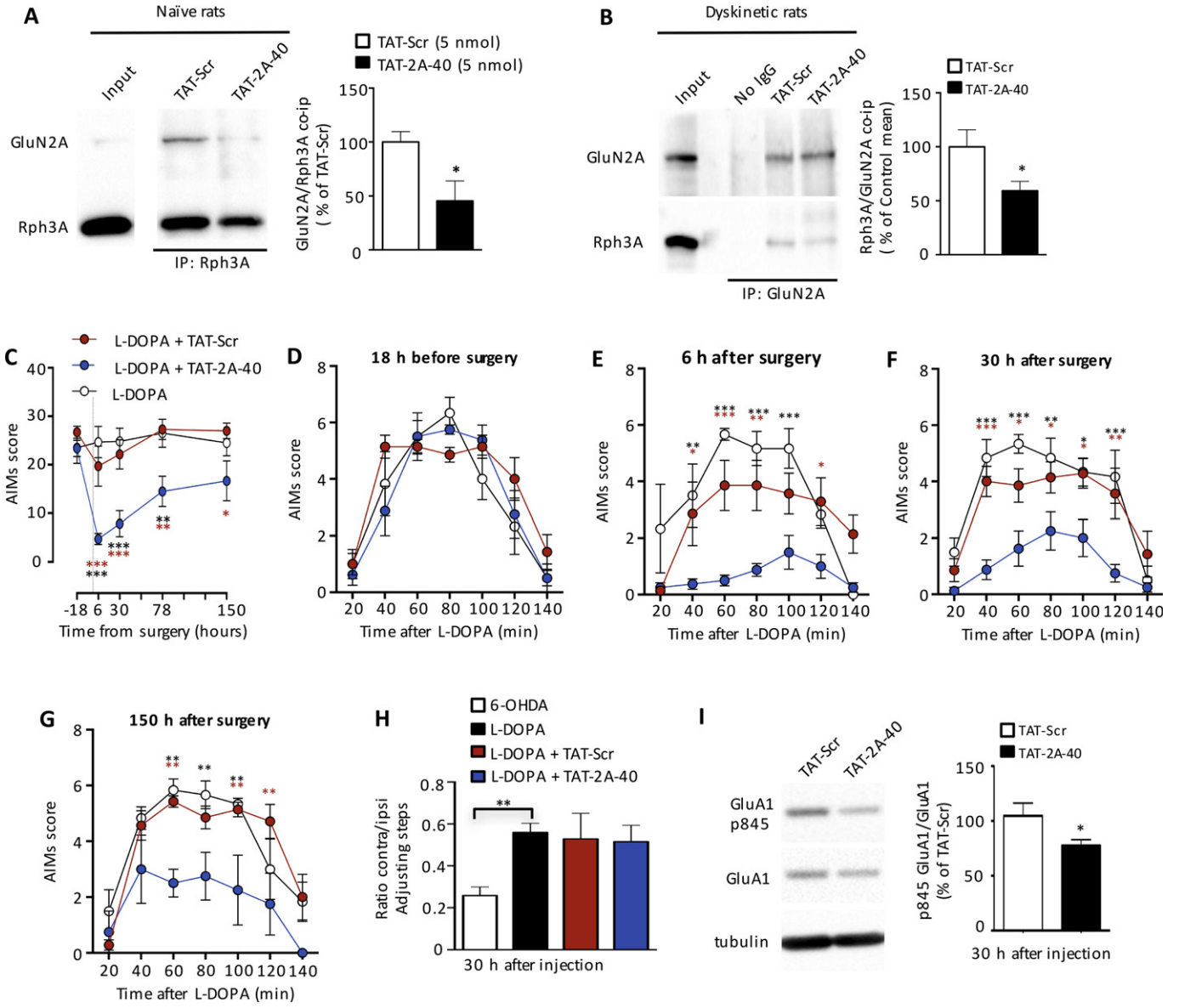


**Fig. 6.** Effect of modulation of GluN2A/Rph3A interaction in 6-OHDA rats displaying dyskinetic behaviour. (A) Coimmunoprecipitation of GluN2A with Rph3A from naïve rats treated 1 h before with TAT-2A-40 (5 nmol) and TAT-Scr (5 nmol). P2 crude membrane fractions were immunoprecipitated (IP) with antibody against Rph3A and the presence of GluN2A in the immunocomplex was evaluated by WB. Treatment with TAT-2A-40 reduces GluN2A co-precipitation with Rph3A (*t*-test, $^{*}p < 0.05$). (B) Coimmunoprecipitation of GluN2A with Rph3A in the striatum from dyskinetic animals at 30 h after TAT-2A-40 and TAT-Scr i.s. injection (5 nmol). P2 crude membrane fractions were immunoprecipitated (IP) with an antibody against GluN2A and the presence of Rph3A in the immunocomplex was evaluated by WB. Treatment with TAT-2A-40 reduces Rph3A co-precipitation with GluN2A (*t*-test, $^{*}p \leq 0.05$). (C) Decrease in the dyskinesia score (AIMs) of 6-OHDA rats treated with L-DOPA after 6 h, 30 h, 78 h and 150 h from the intrastriatal injection of TAT-2A-40 (two-way ANOVA $F_{(8,86)} = 2.186$, $^{*}p = 0.0364$; Tukey post hoc test, 6 h: $^{***}p < 0.001$, L-DOPA - TAT-Scr versus L-DOPA - TAT-2A-40, $^{***}p < 0.001$, L-DOPA - TAT-2A-40 versus L-DOPA; 30 h: $^{***}p < 0.001$, L-DOPA - TAT-Scr versus L-DOPA - TAT-2A-40, $^{***}p < 0.001$, L-DOPA - TAT-2A-40 versus L-DOPA; 78 h: $^{**}p < 0.01$, L-DOPA - TAT-Scr versus L-DOPA - TAT-2A-40, $^{**}p < 0.01$, L-DOPA - TAT-2A-40 versus L-DOPA; 150 h: $^{*}p < 0.05$, L-DOPA - TAT-Scr versus L-DOPA - TAT-2A-40) or TAT-Scr. (D-G) Reduction of AIMs induction in TAT-2A-40 and TAT-Scr injected animals in the session test 18 h before (D) and 6 h (E; two-way ANOVA $F_{(12, 108)} = 3.850$, $^{***}p < 0.0001$; Tukey post hoc test, 40 min: $^{*}p < 0.05$, L-DOPA - TAT-Scr versus L-DOPA - TAT-2A-40, $^{**}p < 0.01$, L-DOPA - TAT-2A-40 versus L-DOPA; 60 min: $^{***}p < 0.001$, L-DOPA - TAT-Scr versus L-DOPA - TAT-2A-40, $^{***}p < 0.001$, L-DOPA - TAT-2A-40 versus L-DOPA; 80 min: $^{**}p < 0.01$, L-DOPA - TAT-Scr versus L-DOPA - TAT-2A-40, $^{***}p < 0.001$, L-DOPA - TAT-2A-40 versus L-DOPA; 100 min: $^{***}p < 0.001$, L-DOPA - TAT-2A-40 versus L-DOPA; 120 min: $^{*}p < 0.05$, L-DOPA - TAT-Scr versus L-DOPA - TAT-2A-40), 30 h (F; two-way ANOVA $F_{(12, 108)} = 2.798$, $^{**}p = 0.0023$; Tukey post hoc test, 40 min: $^{***}p < 0.001$, L-DOPA - TAT-Scr versus L-DOPA - TAT-2A-40, $^{***}p < 0.001$, L-DOPA - TAT-2A-40 versus L-DOPA; 60 min: $^{*}p < 0.05$, L-DOPA - TAT-Scr versus L-DOPA - TAT-2A-40, $^{***}p < 0.001$, L-DOPA - TAT-2A-40 versus L-DOPA; 80 min: $^{*}p < 0.05$, L-DOPA - TAT-Scr versus L-DOPA - TAT-2A-40, $^{**}p < 0.01$, L-DOPA - TAT-2A-40 versus L-DOPA; 100 min: $^{*}p < 0.05$, L-DOPA - TAT-Scr versus L-DOPA - TAT-2A-40, $^{*}p < 0.05$, L-DOPA - TAT-2A-40 versus L-DOPA; 120 min: $^{**}p < 0.01$, L-DOPA - TAT-Scr versus L-DOPA - TAT-2A-40, $^{***}p < 0.001$, L-DOPA - TAT-2A-40 versus L-DOPA), 150 h (G; two-way repeated measures ANOVA $F_{(12, 84)} = 2.762$, $^{**}p = 0.0033$; Tukey post hoc test, 60 min: $^{**}p < 0.01$, L-DOPA - TAT-Scr versus L-DOPA - TAT-2A-40, $^{**}p < 0.01$, L-DOPA - TAT-2A-40 versus L-DOPA; 80 min: $^{**}p < 0.01$, L-DOPA - TAT-2A-40 versus L-DOPA; 100 min: $^{**}p < 0.01$, L-DOPA - TAT-Scr versus L-DOPA - TAT-2A-40, $^{**}p < 0.01$, L-DOPA - TAT-2A-40 versus L-DOPA; 120 min: $^{**}p < 0.01$, L-DOPA - TAT-Scr versus L-DOPA - TAT-2A-40) after CPP injection compared to animals treated only with L-DOPA. (H) The histogram shows the ratio contra/ipsi adjusting steps measured with the stepping test performed 30 h after treatment treatment with TAT-2A-40 and TAT-Scr treated animals. (I) Striatal postsynaptic TIF fractions from TAT-2A-40 and TAT-Scr treated animals were analysed by WB with GluA1 and GluA1-p845 antibodies. The histogram shows quantification of GluA1-p845/GluA1 ratio in the striatal TIF as percentage of TAT-Scr animals (*t*-test, $^{*}p < 0.05$).

addition, it is well-known that NMDARs are overactivated in dyskinetic rats leading to aberrant calcium influx at dendritic spines of striatal MSNs and the onset of pathological synaptic plasticity (Bastide et al. 2015). Interestingly, we recently showed that the concomitant presence of calcium and IP3 induces a dramatic increase of Rph3A binding to GluN2A (Stanic et al. 2015), indicating that both calcium and IP3 are necessary for an efficient molecular recognition mechanism (Coudevylle et al. 2008; Guillen et al. 2013; Montville et al., 2007).

Accordingly, the concomitant high levels of calcium and IP3 in the postsynaptic compartment of glutamatergic corticostriatal synapses together with the increased postsynaptic levels of Rph3A can foster the aberrant Rph3A/GluN2A complex formation observed in dyskinetic rats.

A direct molecular interaction and a functional cross-talk between D1 receptors and NMDARs in dendritic spines of MSNs have been reported (Fiorentini et al. 2003; Jocoy et al. 2011; Ladepeche et al. 2013). We previously demonstrated that D1 receptor activation obtained with a classical receptor agonist, SKF38393, determines a significant decrease of synaptic GluN2A-containing receptors (Vastagh et al. 2012). Interestingly, here we show that D1 but not D2 receptor activation modulates Rph3A synaptic localization, its Ser234 phosphorylation and its interaction with GluN2A-containing NMDARs. In addition, our data show that Ser234-Rph3A phosphorylation is reduced in dyskinetic rats compared to controls thus suggesting that this post-translational modification could be involved in the alteration of Rph3A synaptic localization observed in dyskinetic animals. Notably, it is well-known that the phosphorylated form of Rph3A has a reduced affinity for membranes (Fykse et al. 1995; Foletti et al. 2001) thus suggesting a possible explanation for the enriched accumulation of the protein at the postsynaptic membrane in dyskinetic rats.

Several observations converge in defining Rph3A as a pre- and postsynaptic protein, involved in the regulation of protein localization at synapses. Indeed, Rph3A directly binds proteins including the MAGUK protein CASK and MyoVa, which are localized both in the pre- or postsynaptic compartments and regulate protein trafficking (Brozzi et al. 2012). We recently demonstrated that Rph3A is required for synaptic retention of GluN2A-containing NMDARs at the postsynaptic membrane through the formation of a ternary complex with PSD-95 (Stanic et al. 2015). In particular, Rph3A is responsible for the strengthening of the otherwise weak GluN2A/PSD-95 complex (Stanic et al. 2015; Gardoni et al. 2001). Notably, we previously showed that interfering with the formation of GluN2A/PSD-95 complex leads to a reduction in the dyskinetic motor behaviour in rodent and monkey models of LIDs (Gardoni et al. 2012; Mellone et al. 2015). Overall, these studies indicate that an intervention on PSD-95 function is an efficient strategy to reduce LIDs at least in experimental models. However, considering the large number of protein-protein interactions involving PSD-95 at the excitatory synapse, a direct action on this scaffold protein does not represent an ideal pharmacological approach because of problems of specificity and risk of undesired side effects. Conversely, being PSD-95 and GluN2A the only known partners for Rph3A at the postsynaptic compartment, interfering with GluN2A/PSD-95/Rph3A protein complex could lead to a more specific and direct approach tackling the aberrant NMDAR localization and function in LIDs.

## Acknowledgements

We thank the Electron Microscopy Research Services, Faculty of Medical Sciences, Newcastle University.

## Funding sources

This work was supported by the Cariplo Foundation contract 0660-2014, Progetto di Ricerca di Interesse Nazionale (PRIN2010AHHP5H; PRIN2015FNWP34), Progetto Giovani Ricercatori Ministero Sanità` 2008, Ricerca Finalizzata 2013-02356215, “Investissements d'avenir” ANR-10-IAIHU-06, Umberto Veronesi Foundation Post-doctoral fellowship – Grants 2015, LABEX BRAIN (ANR-10-LABX-43) and Fondation de France. Sponsors had no role in study design, data collection/analysis/interpretation, decision to publish, or preparation of the manuscript.

## Conflict of interest

EB has equity stake in Motac holding Ltd. and receives consultancy payments from Motac Neuroscience Ltd. Current grant support includes Agence Nationale de la Recherche (EB), China Science Fund (EB), IMI (EB), MJFF (EB), France Parkinson (EB), Fondation de France (EB), Medical Research Council (EB). QL is an employee of Motac Neuroscience Ltd.

## References

Ahmed, M., Berthet, A., Bychkov, E., Porras, G., Li, Q., Bioulac, B.H., Carl, Y.T., Bloch, B., Kook, S., Aubert, I., Dovero, S., Doudnikoff, E., Gurevich, V.V., Gurevich, E.V., Bezard, E., 2010. Lentiviral overexpression of GRK6 alleviates L-dopa-induced dyskinesia in experimental Parkinson's disease. Sci. Transl. Med. 2, 28ra28.

Bastide, M.F., Meissner, W.G., Picconi, B., Fasano, S., Fernagut, P.O., Feyder, M., Francardo, V., Alcacer, C., Ding, Y., Brambilla, R., Fisone, G., Jon Stoessl, A., Bourdenx, M., Engeln, M., Navailles, S., De Deurwaerdère, P., Ko, W.K., Simola, N., Morelli, M., Groc, L., Rodriguez, M.C., Gurevich, E.V., Quik, M., Morari, M., Mellone, M., Gardoni, F., Tronci, E., Guehl, D., Tison, F., Crossman, A.R., Kang, U.J., Steece-Collier, K., Fox, S., Carta, M., Angela Cenci, M., Bézard, E., 2015. Pathophysiology of L-dopa-induced motor and non-motor complications in Parkinson's disease. Prog. Neurobiol. 132, 96–168.

Brozzi, F., Diraison, F., Lajus, S., Rajatileka, S., Philips, T., Regazzi, R., Fukuda, M., Verkade, P., Molnár, E., Váradi, A., 2012. Molecular mechanism of myosin Va recruitment to dense core secretory granules. Traffic 13, 54–69.

Burns, M.E., Sasaki, T., Takai, Y., Augustine, G.J., 1998. Rabphilin-3A: a multifunctional regulator of synaptic vesicle traffic. J. Gen. Physiol. 111, 243–255.

Calabresi, P., Pisani, A., Rothwell, J., Ghiglieri, V., Obeso, J.A., Picconi, B., 2016. Hyperkinetic disorders and loss of synaptic downscaling. Nat. Neurosci. 19, 868–875.

Cenci, M.A., Lee, C.S., Björklund, A., 1998. L-DOPA-induced dyskinesia in the rat is associated with striatal overexpression of prodynorphin and glutamic acid decarboxylase mRNA. Eur. J. Neurosci. 10, 2694–2706.

Chung, C.Y., Koprich, J.B., Siddiqi, H., Isacson, O., 2009. Dynamic changes in presynaptic and axonal transport proteins combined with striatal neuroinflammation precede dopaminergic neuronal loss in a rat model of AAV alpha-synucleinopathy. J. Neurosci. 29, 3365–3373.

Coudevylle, N., Montaville, P., Leonov, A., Zweckstetter, M., Becker, S., 2008. Structural determinants for $Ca^{2+}$ and phosphatidylinositol 4,5-bisphosphate binding by the C2A domain of rabphilin-3A. J. Biol. Chem. 283, 35918–35928.

Da Silva-Júnior, F.P., Braga-Neto, P., Sueli Monte, F., de Bruin, V.M., 2005. Amantadine reduces the duration of levodopa-induced dyskinesia: a randomized, double-blind, placebo-controlled study. Parkinsonism Relat. Disord. 11, 449–452.

Dalfó, E., Barrachina, M., Rosa, J.L., Ambrosio, S., Ferrer, I., 2004. Abnormal alpha-synuclein interactions with rab3a and rabphilin in diffuse Lewy body disease. Neurobiol. Dis. 16, 92–97.

Errico, F., Bonito-Oliva, A., Bagetta, V., Vitucci, D., Romano, R., Zianni, E., Napolitano, F., Marinucci, S., Di Luca, M., Calabresi, P., Fisone, G., Carta, M., Picconi, B., Gardoni, F., Usiello, A., 2011. Higher free D-aspartate and N-methyl-D-aspartate levels prevent striatal depotentiation and anticipate L-DOPA-induced dyskinesia. Exp. Neurol. 232, 240–250.

Fernagut, P.O., Li, Q., Dovero, S., Chan, P., Wu, T., Ravenscroft, P., Hill, M., Chen, Z., Bezard, E., 2010. Dopamine transporter binding is unaffected by L-DOPA administration in normal and MPTP-treated monkeys. PLoS One 5, e14053.

Fieblinger, T., Sebastianutto, I., Alcacer, C., Bimpisidis, Z., Maslava, N., Sandberg, S., Engblom, D., Cenci, M.A., 2014. Mechanisms of dopamine D1 receptor-mediated ERK1/2 activation in the parkinsonian striatum and their modulation by metabotropic glutamate receptor type 5. J. Neurosci. 34, 4728–4740.

Fiorentini, C., Gardoni, F., Spano, P., Di Luca, M., Missale, C., 2003. Regulation of dopamine D1 receptor trafficking and desensitization by oligomerization with glutamate N-methyl-D-aspartate receptors. J. Biol. Chem. 278, 20196–20202.

Foletti, D.L., Blitzer, J.T., Scheller, R.H., 2001. Physiological modulation of rabphilin phosphorylation. J. Neurosci. 21, 5473–5483.

Fykse, E.M., Li, C., Sudhof, T.C., 1995. Phosphorylation of rabphilin-3A by Ca2+/calmodulin- and cAMP-dependent protein kinases in vitro. J. Neurosci. 15, 2385–2395.

Gardoni, F., Di Luca, M., 2015. Targeting glutamatergic synapses in Parkinson's disease. Curr. Opin. Pharmacol. 20, 24–28.

Gardoni, F., Schrama, L.H., Kamal, A., Gispen, W.H., Cattabeni, F., Di Luca, M., 2001. Hippocampal synaptic plasticity involves competition between Ca2+/calmodulin-dependent protein kinase II and postsynaptic density 95 for binding to the NR2A subunit of the NMDA receptor. J. Neurosci. 21, 1501–1509.

Gardoni, F., Picconi, B., Ghiglieri, V., Polli, F., Bagetta, V., Bernardi, G., Cattabeni, F., Di Luca, M., Calabresi, P., 2006. A critical interaction between NR2B and MAGUK in L-DOPA induced dyskinesia. J. Neurosci. 26, 2914–2922.

Gardoni, F., Sgobio, C., Pendolino, V., Calabresi, P., Di Luca, M., Picconi, B., 2012. Targeting NR2A-containing NMDA receptors reduces L-DOPA-induced dyskinesias. Neurobiol. Aging 33, 2138–2144.

Ghiglieri, V., Mineo, D., Vannelli, A., Cacace, F., Mancini, M., Pendolino, V., Napolitano, F., Di Maio, A., Mellone, M., Stanic, J., Tronci, E., Fidalgo, C., Stancampiano, R., Carta, M., Calabresi, P., Gardoni, F., Usiello, A., Picconi, B., 2016. Modulation of serotoninergic transmission by eltoprazine in L-DOPA-induced dyskinesia: behavioral, molecular, and synaptic mechanisms. Neurobiol. Dis. 86, 140–153.

Guillen, J., Ferrer-Orta, C., Buxaderas, M., Pérez-Sánchez, D., Guerrero-Valero, M., Luengo-Gil, G., Pous, J., Guerra, P., Gómez-Fernández, J.C., Verdaguer, N., Corbalán-García, S., 2013. Structural insights into the $Ca^{2+}$ and PI(4,5)P2 binding modes of the C2 domains of rabphilin 3A and synaptotagmin 1. Proc. Natl. Acad. Sci. U. S. A. 110, 20503–20508.

Hill, M.D., Martin, R.H., Mikulis, D., Wong, J.H., Silver, F.L., Terbrugge, K.G., Milot, G., Clark, W.M., Macdonald, R.L., Kelly, M.E., Boulton, M., Fleetwood, I., McDougall, C., Gunnarsson, T., Chow, M., Lum, C., Dodd, R., Poublanc, J., Krings, T., Demchuk, A.M., Goyal, M., Anderson, R., Bishop, J., Garman, D., Tymianski, M., ENACT trial

investigators., 2012. Safety and efficacy of NA-1 in patients with iatrogenic stroke after endovascular aneurysm repair (ENACT): a phase 2, randomized, double-blind, placebo-controlled trial. Lancet Neurol. 11, 942–950.
Jocoy, E.L., André, V.M., Cummings, D.M., Rao, S.P., Wu, N., Ramsey, A.J., Caron, M.G., Cepeda, C., Levine, M.S., 2011. Dissecting the contribution of individual receptor subunits to the enhancement of Nmethyl-D-aspartate currents by dopamine D1 receptor activation in striatum. Front. Syst. Neurosci. 5, 28.
Kornhuber, J., Bormann, J., Hübers, M., Rusche, K., Riederer, P., 1991. Effects of the 1-amino-adamantanes at the MK-801-binding site of the NMDA-receptor-gated ion channel: a human postmortem brain study. Eur. J. Pharmacol. 206, 297–300.
Ladepeche, L., Dupuis, J.P., Bouchet, D., Doudnikoff, E., Yang, L., Campagne, Y., Bézard, E., Hosy, E., Groc, L., 2013. Single-molecule imaging of the functional crosstalk between surface NMDA and dopamine D1 receptors. Proc. Natl. Acad. Sci. U. S. A. 110, 18005–18010.
Luginger, E., Wenning, G.K., Bösch, S., Poewe, W., 2000. Beneficial effects of amantadine on L-dopa-induced dyskinesias in Parkinson's disease. Mov. Disord. 15, 873–878.
Lundblad, M., Andersson, M., Winkler, C., Kirik, D., Wierup, N., Cenci, M.A., 2002. Pharmacological validation of behavioural measures of akinesia and dyskinesia in a rat model of Parkinson's disease. Eur. J. Neurosci. 15, 120–132.
Medvedev, I.O., Ramsey, A.J., Masoud, S.T., Bermejo, M.K., Urs, N., Sotnikova, T.D., Beaulieu, J.M., Gainetdinov, R.R., Salahpour, A., 2013. D1 dopamine receptor coupling to PLCβ regulates forward locomotion in mice. J. Neurosci. 33, 18125–18133.
Mellone, M., Gardoni, F., 2013. Modulation of NMDA receptor at the synapse: promising therapeutic interventions in disorders of the nervous system. Eur. J. Pharmacol. 719, 75–83.
Mellone, M., Stanic, J., Hernandez, L.F., Iglesias, E., Zianni, E., Longhi, A., Prigent, A., Picconi, B., Calabresi, P., Hirsch, E.C., Obeso, J.A., Di Luca, M., Gardoni, F., 2015. NMDA receptor GluN2A/GluN2B subunit ratio as synaptic trait of levodopa-induced dyskinesias: from experimental models to patients. Front. Cell. Neurosci. 9, 245.
Moreau, M.M., Piguel, N., Papouin, T., Koehl, M., Durand, C.M., Rubio, M.E., Loll, F., Richard, E.M., Mazzocco, C., Racca, C., Oliet, S.H., Abrous, D.N., Montcouquiol, M., Sans, N., 2010. The planar polarity protein Scribble1 is essential for neuronal plasticity and brain function. J. Neurosci. 30, 9738–9752.
Ory-Magne, F., Corvol, J.C., Azulay, J.P., Bonnet, A.M., Brefel-Courbon, C., Damier, P., Dellapina, E., Destée, A., Durif, F., Galitzky, M., Lebouvier, T., Meissner, W., Thalamas, C., Tison, F., Salis, A., Sommet, A., Viallet, F., Vidailhet, M., Rascol, O., NS-Park CIC Network, 2014. Withdrawing amantadine in dyskinetic patients with Parkinson disease: the AMANDYSK trial. Neurology 82, 300–307.
Paillé, V., Picconi, B., Bagetta, V., Ghiglieri, V., Sgobio, C., Di Filippo, M., Viscomi, M.T., Giampà, C., Fusco, F.R., Gardoni, F., Bernardi, G., Greengard, P., Di Luca, M., Calabresi, P., 2010. Distinct levels of dopamine denervation differentially alter striatal synaptic plasticity and NMDA receptor subunit composition. J. Neurosci. 30, 14182–14193.
Paoletti, P., Bellone, C., Zhou, Q., 2013. NMDA receptor subunit diversity: impact on receptor properties, synaptic plasticity and disease. Nat. Rev. Neurosci. 14, 383–400.
Piguel, N.H., Fievre, S., Blanc, J.M., Carta, M., Moreau, M.M., Moutin, E., Pinheiro, V.L., Medina, C., Ezan, J., Lasvaux, L., Loll, F., Durand, C.M., Chang, K., Petralia, R.S., Wenthold, R.J., Stephenson, F.A., Vuillard, L., Darbon, H., Perroy, J., Mulle, C., Montcouquiol, M., Racca, C., Sans, N., 2014. Scribble1/AP2 complex coordinates NMDA receptor endocytic recycling. Cell Rep. 9, 712–727.
Porras, G., Berthet, A., Dehay, B., Li, Q., Ladepeche, L., Normand, E., Dovero, S., Martinez, A., Doudnikoff, E., Martin-Négrier, M.L., Chuan, Q., Bloch, B., Choquet, D., Boué-Grabot, E., Groc, L., Bezard, E., 2012. PSD-95 expression controls L-DOPA dyskinesia through dopamine D1 receptor trafficking. J. Clin. Invest. 122, 3977–3989.
Santini, E., Sgambato-Faure, V., Li, Q., Savasta, M., Dovero, S., Fisone, G., Bezard, E., 2010. Distinct changes in cAMP and extracellular signal-regulated protein kinase signalling in L-DOPA-induced dyskinesia. PLoS One 5, e12322.
Shen, W., Plotkin, J.L., Francardo, V., Ko, W.K., Xie, Z., Li, Q., Fieblinger, T., Wess, J., Neubig, R.R., Lindsley, C.W., Conn, P.J., Greengard, P., Bezard, E., Cenci, M.A., Surmeier, D.J., 2015. M4 muscarinic receptor signaling ameliorates striatal plasticity deficits in models of L-DOPA-induced dyskinesia. Neuron 88, 762–773.
Smith, R., Petersén, A., Bates, G.P., Brundin, P., Li, J.Y., 2005. Depletion of rabphilin 3A in a transgenic mouse model (R6/1) of Huntington's disease, a possible culprit in synaptic dysfunction. Neurobiol. Dis. 20, 673–684.
Smith, R., Klein, P., Koc-Schmitz, Y., Waldvogel, H.J., Faull, R.L., Brundin, P., Plomann, M., Li, J.Y., 2007. Loss of SNAP-25 and rabphilin 3a in sensory-motor cortex in Huntington's disease. J. Neurochem. 103, 115–123.
Snow, B.J., Macdonald, L., Mcauley, D., Wallis, W., 2000. The effect of amantadine on levodopa-induced dyskinesias in Parkinson's disease: a double-blind, placebo-controlled study. Clin. Neuropharmacol. 23, 82–85.
Stanic, J., Carta, M., Eberini, I., Pelucchi, S., Marcello, E., Genazzani, A.A., Racca, C., Mulle, C., Di Luca, M., Gardoni, F., 2015. Rabphilin 3A retains NMDA receptors at synaptic sites through interaction with GluN2A/PSD-95 complex. Nat. Commun. 6, 10181.
Tan, M.G., Lee, C., Lee, J.H., Francis, P.T., Williams, R.J., Ramírez, M.J., Chen, C.P., Wong, P.T., Lai, M.K., 2014. Decreased rabphilin 3A immunoreactivity in Alzheimer's disease is associated with Aβ burden. Neurochem. Int. 64, 29–36.
Thomas, A., Iacono, D., Luciano, A.L., Armellino, K., Di Iorio, A., Onofrj, M., 2004. Duration of amantadine benefit on dyskinesia of severe Parkinson's disease. J. Neurol. Neurosurg. Psychiatry 75, 141–143.
Urs, N.M., Bido, S., Peterson, S.M., Daigle, T.L., Bass, C.E., Gainetdinov, R.R., Bezard, E., Caron, M.G., 2015. Targeting beta-arrestin2 in the treatment of L-DOPA-induced dyskinesia in Parkinson's disease. Proc. Natl. Acad. Sci. U. S. A. 112, E2517–2526.
Vastagh, C., Gardoni, F., Bagetta, V., Stanic, J., Zianni, E., Giampà, C., Picconi, B., Calabresi, P., Di Luca, M., 2012. N-methyl-D-aspartate (NMDA) receptor composition modulates dendritic spine morphology in striatal medium spiny neurons. J. Biol. Chem. 287, 18103–18114.
Wolf, E., Seppi, K., Katzenschlager, R., Ransmayr, G., Schwingenschuh, P., Ott, E., Kloiber, I., Haubenberger, D., Auff, E., Poewe, W., 2010. Long-term antidyskinetic efficacy of amantadine in Parkinson's disease. Mov. Disord. 25, 1357–1363.